Contributions of Transition and Parametric X-Ray Radiation along the Relativistic Electron Velocity in the Laue Geometry

S. V. Blazhevich[a] and A. V. Noskov[b]

[a] *Belgorod State University, Belgorod, Russia*

[b] *Belgorod University of Consumer Cooperation, Belgorod, Russia*

Received August 10, 2009

Abstract—Parametric X-radiation along the velocity of a relativistic electron (FPXR) moving through a single crystal plate is analyzed in the Laue scattering geometry. It is shown that the ratio between the contributions of these radiation mechanisms strongly depends on the degree of reflection asymmetry. The presented theoretical results can be used for experimental investigations of FPXR.

INTRODUCTION

When a fast charged particle moves through a single crystal, its Coulomb field is scattered by parallel crystalline atomic planes of the crystal, generating parametric X-radiation (PXR) [1–3]. The theory of PXR from a relativistic particle in the crystal predicts that radiation can be emitted not only in the direction of Bragg scattering, but also along the velocity of the emitting particle (FPXR) [4–6]. This radiation is caused by the dynamic diffraction effects of PXR. Attempts to perform experimental studies of FPXR are known [7–11]. However, the first report of an experimental observation of FPXR appeared only recently, in [10]. In this experiment, transition radiation in neighborhood of Bragg frequency was suppressed via destructive interference of the waves of transition radiation on the input and output surfaces of a crystalline plate. However, in [10], the narrow spectral peak of transition radiation caused by the dynamic effects, which arises in the neighborhood of Bragg frequency [12], was not analyzed. Nevertheless, this experimental peak could be interpreted as the FPXR peak. In [11], X-radiation of relativistic electrons moving in a thick absorbing single-crystal target was measured under the conditions of generation of FPXR. However, the desired reflection was not clearly distinguishable on the background of radiation produced by electrons of the structural components of the experimental setup. Thus, the theoretical study of the properties of PXR along the particle velocity and search for optimal conditions of reliable experimental observation of this dynamic effect remain urgent problems.

In the case of symmetric reflection, the dynamic effect of FPXR on the background of transition radiation (TR) was described theoretically in [13–15]. In the general case of asymmetric reflection, theoretical descriptions of PXR, transition radiation, and FPXR in the Laue geometry were reported in [16–18]. It has been demonstrated that the spectral-angular densities of the above-mentioned radiations substantially depend on the asymmetry parameter. Effects related to the degree of asymmetry have been revealed.

In this paper, parametric X-radiation along the velocity of a relativistic electron is considered in the Laue scattering geometry in the case in which reflection is asymmetric and atomic planes can be situated at arbitrary angle δ with the target surface. The expressions describing the spectral-angular density of FPXR, TR, and their interference are derived via the two-wave approximation of the dynamic diffraction theory [20].

SPECTRAL-ANGULAR DISTRIBUTION OF RADIATION

Let us consider radiation of a relativistic electron when it moves through a crystalline plate with thickness L at constant velocity $\mathbf{V}$ (Fig. 1). In [21], expressions for describing contributions to the spectral-angular densities of FPXR and TR and the summand characterizing their interference have been derived:

$$\omega\frac{d^2N^{(s)}_{\mathrm{FPXR}}}{d\omega d\Omega} = \frac{e^2}{4\pi^2}P^{(s)^2}\frac{\theta^2}{(\theta^2+\gamma^{-2}-\chi'_0)^2}R^{(s)}_{\mathrm{FPXR}}, \qquad (1a)$$

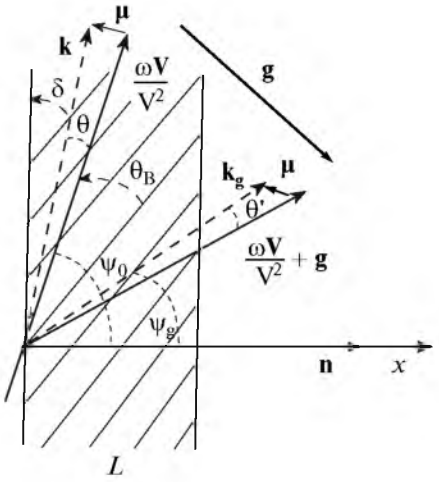

Fig. 1. Geometry of radiation propagation: θ' is the radiation angle, θ_B is the Bragg angle (the angle between electron velocity **V** and atomic planes), δ is the angle between the plate surface and the crystal's atomic planes under consideration, and **k** and $\mathbf{k}_g = \mathbf{k} + \mathbf{g}$ are the wave vectors of incident and diffracted photons.

$$R^{(s)}_{\mathrm{FPXR}} = \frac{4}{\xi^{(s)^2}+\varepsilon}\frac{\sin^2\left(\frac{b^{(s)}}{2}\left(\sigma^{(s)}+\frac{\xi^{(s)}-\sqrt{\xi^{(s)^2}+\varepsilon}}{\varepsilon}\right)\right)}{\left(\sigma^{(s)}+\frac{\xi^{(s)}-\sqrt{\xi^{(s)^2}+\varepsilon}}{\varepsilon}\right)^2}; \quad (1b)$$

$$\omega\frac{d^2N^{(s)}_{\mathrm{TR}}}{d\omega d\Omega} = \frac{e^2}{4\pi^2}P^{(s)^2}\theta^2 \times\left(\frac{1}{\theta^2+\gamma^{-2}}-\frac{1}{\theta^2+\gamma^{-2}-\chi'_0}\right)^2 R^{(s)}_{\mathrm{TR}}, \quad (2a)$$

$$R^{(s)}_{\mathrm{TR}} = 4\left(1-\frac{\xi^{(s)}}{\sqrt{\xi^{(s)^2}+\varepsilon}}\right)^2 \times\sin^2\left(\frac{b^{(s)}}{2}\left(\sigma^{(s)}+\frac{\xi^{(s)}+\sqrt{\xi^{(s)^2}+\varepsilon}}{\varepsilon}\right)\right)+4\left(1+\frac{\xi^{(s)}}{\sqrt{\xi^{(s)^2}+\varepsilon}}\right)^2 \times\sin^2\left(\frac{b^{(s)}}{2}\left(\sigma^{(s)}+\frac{\xi^{(s)}-\sqrt{\xi^{(s)^2}+\varepsilon}}{\varepsilon}\right)\right) +\frac{4\varepsilon}{\xi^{(s)^2}+\varepsilon}\left(\cos^2\left(\frac{b^{(s)}\sqrt{\xi^{(s)^2}+\varepsilon}}{\varepsilon}\right) -\cos\left(b^{(s)}\left(\sigma^{(s)}+\frac{\xi^{(s)}}{\varepsilon}\right)\right)\cos\left(b^{(s)}\left(\frac{\sqrt{\xi^{(s)^2}+\varepsilon}}{\varepsilon}\right)\right)\right). \quad (2b)$$

$$\omega\frac{d^2N^{(s)}_{\mathrm{INT}}}{d\omega d\Omega} = \frac{e^2}{4\pi^2}P^{(s)^2}\theta^2\left(\frac{1}{\theta^2+\gamma^{-2}} -\frac{1}{\theta^2+\gamma^{-2}-\chi'_0}\right)\frac{1}{\theta^2+\gamma^{-2}-\chi'_0}R^{(s)}_{\mathrm{INT}}, \quad (3a)$$

$$R^{(s)}_{\mathrm{INT}} = -\frac{4}{\sqrt{\xi^{(s)^2}+\varepsilon}\left(\sigma^{(s)}+\frac{\xi^{(s)}-\sqrt{\xi^{(s)^2}+\varepsilon}}{\varepsilon}\right)} \times\left[\left(1-\frac{\xi^{(s)}}{\sqrt{\xi^{(s)^2}+\varepsilon}}\right)\cos^2\left(\frac{b^{(s)}\sqrt{\xi^{(s)^2}+\varepsilon}}{\varepsilon}\right) -\cos\left(\frac{b^{(s)}\sqrt{\xi^{(s)^2}+\varepsilon}}{\varepsilon}\right)\cos\left(b^{(s)}\left(\sigma^{(s)}+\frac{\xi^{(s)}}{\varepsilon}\right)\right)\right) +2\left(1+\frac{\xi^{(s)}}{\sqrt{\xi^{(s)^2}+\varepsilon}}\right)\sin^2\left(\frac{b^{(s)}}{2}\left(\sigma^{(s)}+\frac{\xi^{(s)}-\sqrt{\xi^{(s)^2}+\varepsilon}}{\varepsilon}\right)\right)\Bigg]. \quad (3b)$$

As in [21], we introduce the following designations:

$$\xi^{(s)}(\omega) = \eta^{(s)}(\omega)+\frac{1-\varepsilon}{2\nu^{(s)}},$$

$$\eta^{(s)}(\omega) = \frac{2\sin^2\theta_B}{V^2\left|\chi'_g\right|C^{(s)}}\left(1-\frac{\omega(1-\theta\cos\varphi\,\mathrm{ctg}\theta_B)}{\omega_B}\right),$$

$$b^{(s)} = \frac{1}{2\sin(\delta-\theta_B)}\frac{L}{L^{(s)}_{\mathrm{ext}}}, \quad \sigma^{(s)} = \frac{1}{\nu^{(s)}}\left(\frac{\theta^2}{\left|\chi'_0\right|}+\frac{1}{\gamma^2\left|\chi'_0\right|}+1\right), \quad (4)$$

$$\nu^{(s)} = \frac{\chi'_g C^{(s)}}{\chi'_0}.$$

Expression (1)–(3) involves parameter ε that determines the degree of asymmetry:

$$\varepsilon = \frac{\sin(\delta+\theta_B)}{\sin(\delta-\theta_B)}, \quad (5)$$

where θ_B is the angle between the electron velocity and the system of crystal planes.

Note that the angles between the wave vectors of incident and diffracted photons and the plate surface can be equal (symmetric reflection, Fig. 2) or unequal (asymmetric reflection). In addition, $\varepsilon = 1$ and $\delta = \pi/2$ if reflection is symmetric and $\varepsilon \neq 1$ and $\delta \neq \pi/2$ if reflection is asymmetric. The angle of an incident electron with the plate surface, $\delta - \theta_B$, increases with decreasing parameter ε and vice versa (Fig. 2).

Spectral curves constructed according to formula (1b) (Fig. 3) exhibit a growth in the intensity of the FPXR peak and a decrease in its spectral width when crystal thickness increases. It should be noted that FPXR has an interesting property related

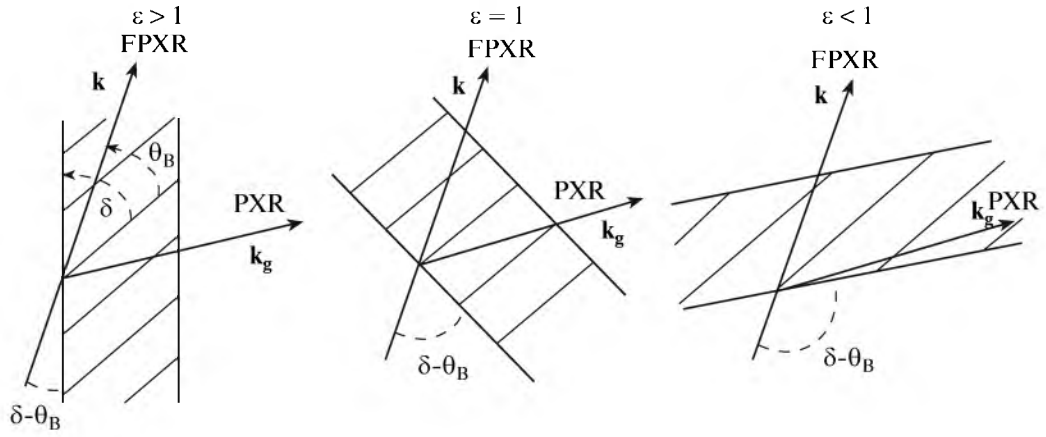

Fig. 2. Radiation reflection from the crystalline plate: ($\varepsilon = 1$) symmetric reflection and ($\varepsilon > 1$, $\varepsilon < 1$) asymmetric reflection.

to the asymmetric reflection of the relativistic electron field from the crystalline plate (with respect to its surface). It turns out that, likewise, the FPXR spectrum peak amplitude substantially increases (Fig. 4) and its spectral width decreases with decreasing asymmetry parameter ε. To highlight this effect, curves corresponding to different values of ε were constructed at the fixed angle θ_B between the electron velocity and parallel diffracting atomic planes of the crystal and for the constant electron path in the crystalline plate, which is characterized by parameter $b^{(s)}$.

Let us consider the influence of asymmetry on the angular density of PXR. For this purpose, expression (1a) is integrated with respect to frequency function $\eta^{(s)}(\omega)$:

$$\frac{dN^{(s)}_{\mathrm{FPXR}}}{d\Omega} = \frac{e^2 \nu^{(s)} P^{(s)^2}}{8\pi^2 \sin^2\theta_B} F^{(s)}_{\mathrm{FPXR}}, \tag{6a}$$

$$F^{(s)}_{\mathrm{FPXR}} = \frac{\dfrac{\theta^2}{\left|\chi_0'\right|}}{\left(\dfrac{\theta^2}{\left|\chi_0'\right|} + \dfrac{1}{\gamma^2\left|\chi_0'\right|} + 1\right)^2} \int_{-\infty}^{+\infty} R^{(s)}_{\mathrm{FPXR}}\, d\eta^{(s)}. \tag{6b}$$

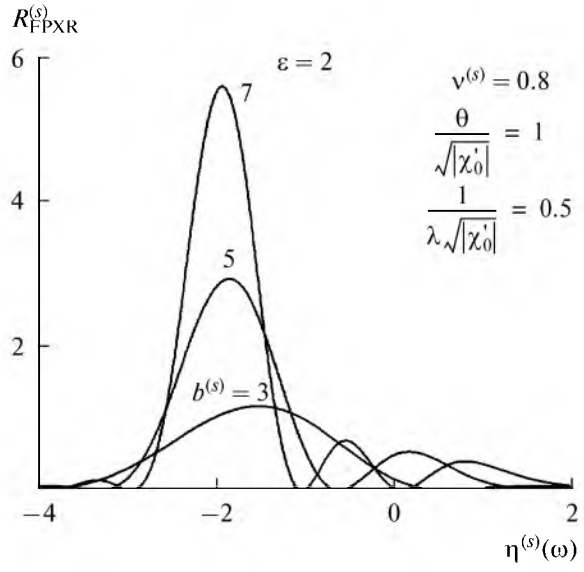

Fig. 3. Comparison of FPXR spectra calculated for different particle paths in the target.

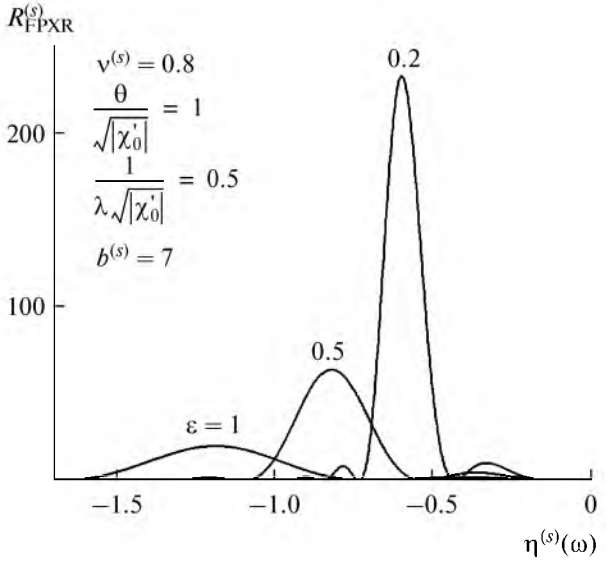

Fig. 4. Comparison of FPXR spectra calculated for different values of the asymmetry parameter.

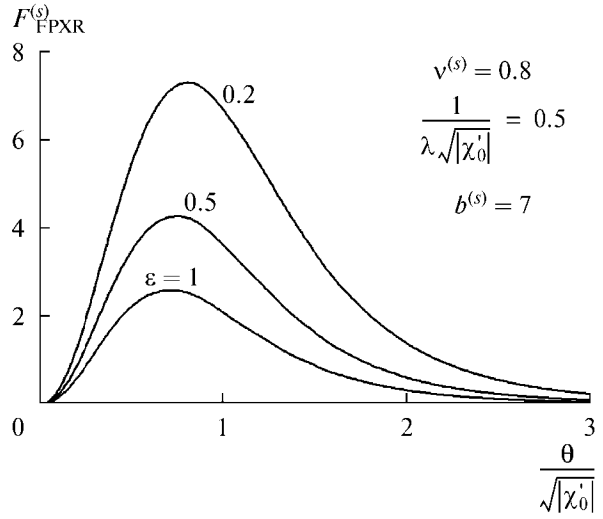

Fig. 5. Influence of reflection asymmetry on the angular density of FPXR.

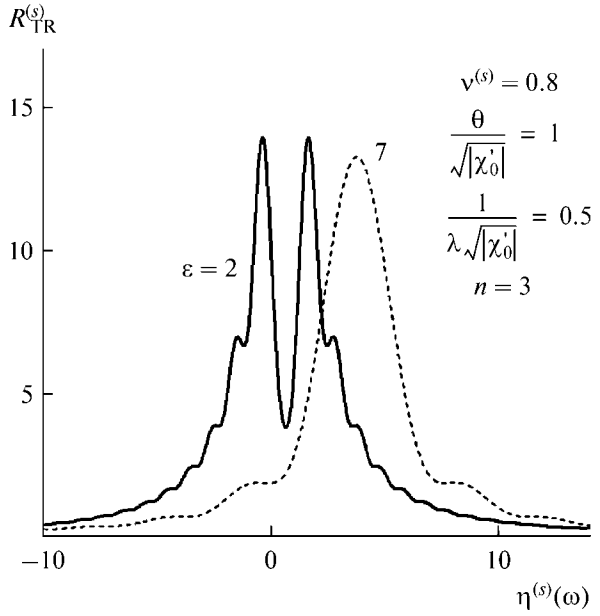

Fig. 6. TR spectra for different values of the asymmetry parameter.

Curves that describe the angular density of FPXR and were constructed according to formula (6b) for different values of reflection asymmetry parameter ε are presented in Fig. 5. They exhibit a significant growth in angular density with decreasing parameter ε. Thus, when θ_B and electron path $2b^{(s)}$ have fixed values, the FPXR spectrum peak amplitude and the angular density substantially depend on angle δ between the surface of the crystalline plate and the system of diffracting atomic planes.

ANALYSIS OF THE CONTRIBUTION OF TR TO THE TOTAL RADIATION YIELD AND THE INFLUENCE OF INTERFERENCE BETWEEN FPXR AND TR

In the real experiment, the contribution of FPXR can be observed only in the presence of TR. Hence, it is necessary to analyze the contribution of TR and interference between FPXR and TR.

Expression (2b) describes the transition radiation spectrum formed on the input and output surfaces of a target. The first two summands correspond to the second and first mechanisms of radiation, and the third summand characterizes their interference.

Distribution (2b) substantially differs from ordinary TR emitted by amorphous dielectric plate with thickness L. This difference caused by the dynamic diffraction effects is observed only in the neighborhood of Bragg frequency ω_B. Beyond this neighborhood $\left(\left|\xi^{(s)}\right| \gg \varepsilon\right)$, function $R^{(s)}_{\mathrm{TR}}$ takes the form of the well-known expression for describing the interference between the waves of TR emitted by the input and output surfaces of the plate,

$$R^{(s)}_{\mathrm{TR}} \approx 16\sin^2\left(\frac{b^{(s)}\sigma^{(s)}}{2}\right) \equiv 16\sin^2\left(\frac{\omega L_e}{4}\left(\theta^2 + \gamma^{-2} - \chi_0'\right)\right), \tag{7}$$

where L_e is the electron path in the plate.

Expression (7) indicates the possibility of decreasing the TR contribution into the total radiation yield in the neighborhood of Bragg frequency by interferential suppression of the contribution of ordinary TR in the sufficiently wide neighborhood of Bragg frequency ω_B for the fixed angle of observation under the condition

$$\frac{b^{(s)}\sigma^{(s)}}{2} = \pi n,\ n = 0, \pm 1, \ldots \tag{8}$$

Functions $R^{(s)}_{\mathrm{ПИ}}$, which were calculated from (2b) for fixed values of parameters $\nu^{(s)}$ and $\frac{1}{\gamma^2|\chi_0'|}$ and different values of asymmetry parameter ε, are presented in Fig. 6. Parameter $b^{(s)}$ and observation angle θ are selected according to resonance condition (8) for $n = 3$. It follows from Fig. 6 that the TR peak shape depends on the reflection asymmetry because the asymmetry parameter affects the ratio between the phase of the TR wave formed on the input surface of a crystalline plate (after the dynamic diffraction in the crystal) and the phase of the TR wave emitted from the output surface of a crystalline target.

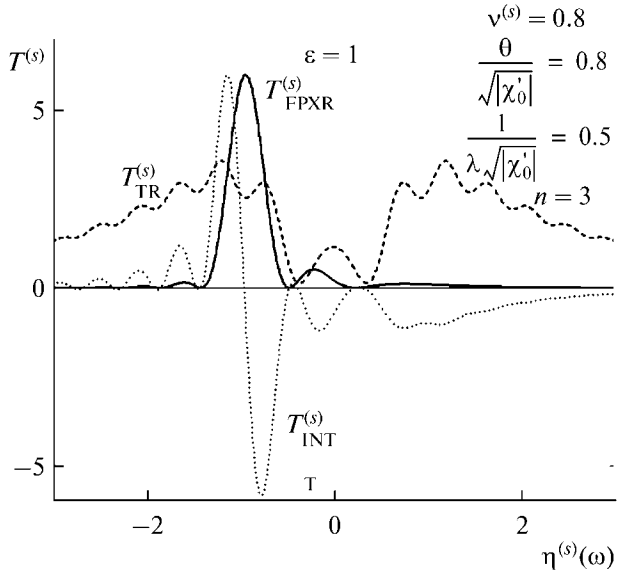

Fig. 7. Relative contributions of FPXR, TR, and their interferential summand in the case of symmetric reflection.

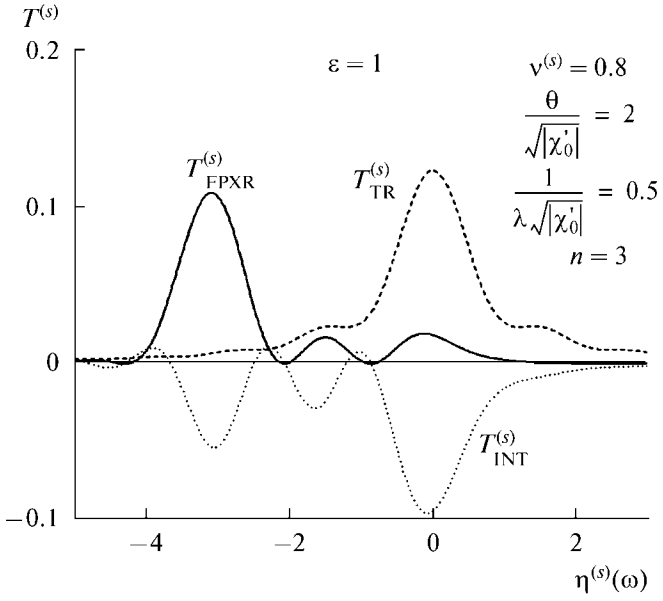

Fig. 8. Relative contributions similar to those in Fig. 7 for another fixed observation angle.

The angular distributions of FPXR and TR are distinguished at a fairly high energy of an emitting particle ($\gamma^2|\chi_0'| \gg 1$). According to expression (2a), the TR angular distribution maximum is located near the angle $\theta \approx \gamma^{-1}$ and FPXR is concentrated near the large angles $\theta \sim \sqrt{|\chi_0'|} \gg \gamma^{-1}$ (Fig. 5). The ratio between the contributions of collimated FPXR and TR strongly depends on observation angle θ. To estimate this ratio, the interference between FPXR and TR must be taken into account.

To analyze the relative contributions of FPXR and TR and its interference expression into the total radiation yield, let us represent expressions (1), (2), and (3) as

$$\omega\frac{d^2N^{(s)}_{\mathrm{FPXR}}}{d\omega d\Omega} = \frac{e^2}{4\pi^2}\frac{P^{(s)^2}}{|\chi_0'|}T^{(s)}_{\mathrm{FPXR}},$$

$$T^{(s)}_{\mathrm{FPXR}} = \frac{\dfrac{\theta^2}{|\chi_0'|}}{\left(\dfrac{\theta^2}{|\chi_0'|} + \dfrac{1}{\gamma^2|\chi_0'|} + 1\right)^2}R^{(s)}_{\mathrm{FPXR}}, \qquad (9)$$

$$\omega\frac{d^2N^{(s)}_{\mathrm{TR}}}{d\omega d\Omega} = \frac{e^2}{4\pi^2}\frac{P^{(s)^2}}{|\chi_0'|}T^{(s)}_{\mathrm{TR}},$$

$$T^{(s)}_{\mathrm{TR}} = \frac{\dfrac{\theta^2}{|\chi_0'|}}{\left(\dfrac{\theta^2}{|\chi_0'|} + \dfrac{1}{\gamma^2|\chi_0'|} + 1\right)^2\left(\dfrac{\theta^2}{|\chi_0'|} + \dfrac{1}{\gamma^2|\chi_0'|}\right)^2}R^{(s)}_{\mathrm{TR}}, \qquad (10)$$

$$\omega\frac{d^2N^{(s)}_{\mathrm{INT}}}{d\omega d\Omega} = \frac{e^2}{4\pi^2}\frac{P^{(s)^2}}{|\chi_0'|}T^{(s)}_{\mathrm{INT}},$$

$$T^{(s)}_{\mathrm{INT}} = \frac{\dfrac{\theta^2}{|\chi_0'|}}{\left(\dfrac{\theta^2}{|\chi_0'|} + \dfrac{1}{\gamma^2|\chi_0'|} + 1\right)^2\left(\dfrac{\theta^2}{|\chi_0'|} + \dfrac{1}{\gamma^2|\chi_0'|}\right)}R^{(s)}_{\mathrm{INT}}. \qquad (11)$$

Spectral-angular distributions for FPXR and TR and their interferential summand are presented in Figs. 7 and 8. The relative contributions were calculated according to formulas (9)–(11) for different fixed observation angles under the assumption that condition (8) is satisfied. It should be noted that the FPXR and TR peaks have a small width (on the order of several eV). The presented curves constructed for symmetric reflection ($\varepsilon = 1$) show that the interference between FPXR and TR substantially affects the total radiation spectrum. In addition, only TR contributes to the formation of a narrow spectral peak in the range of small observation angles, as seen in Fig. 7. The relative contribution of PXR grows with increas-

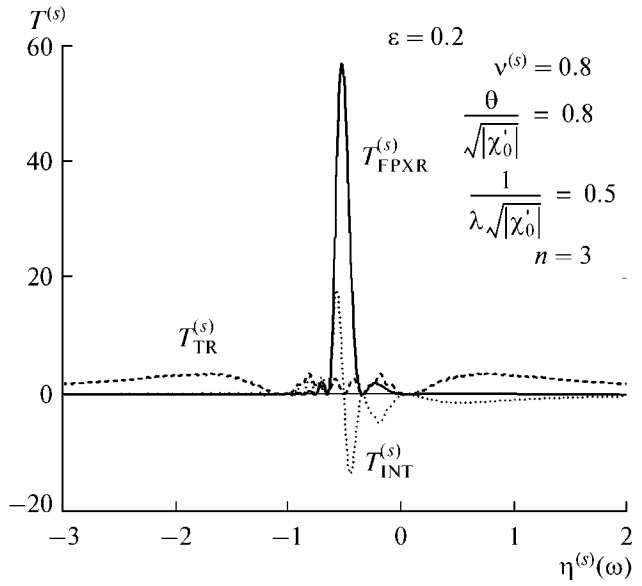

Fig. 9. Relative contributions similar to those in Fig. 7 in the case of asymmetric reflection.

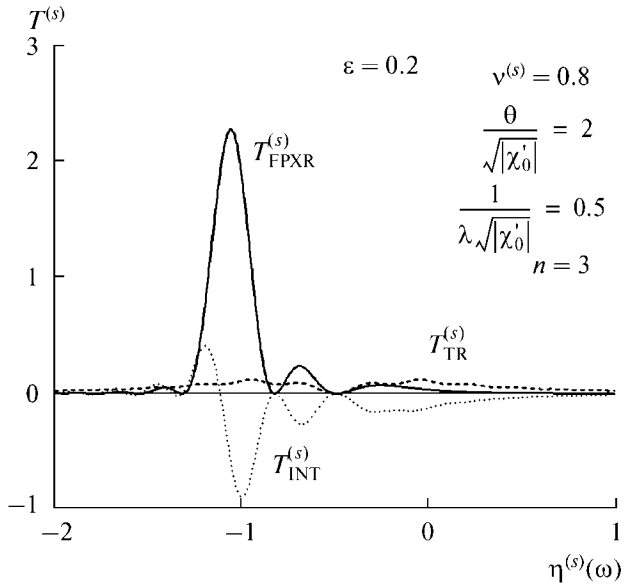

Fig. 10. Relative contributions similar to those in Fig. 8 in the case of asymmetric reflection.

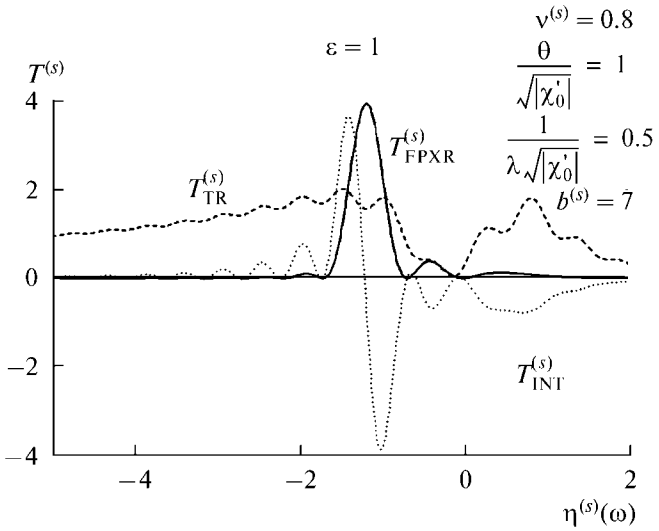

Fig. 11. Relative contributions of FPXR, TR, and the interferential expression into the total radiation yield in the case where reflection is symmetric and condition (8) is not satisfied.

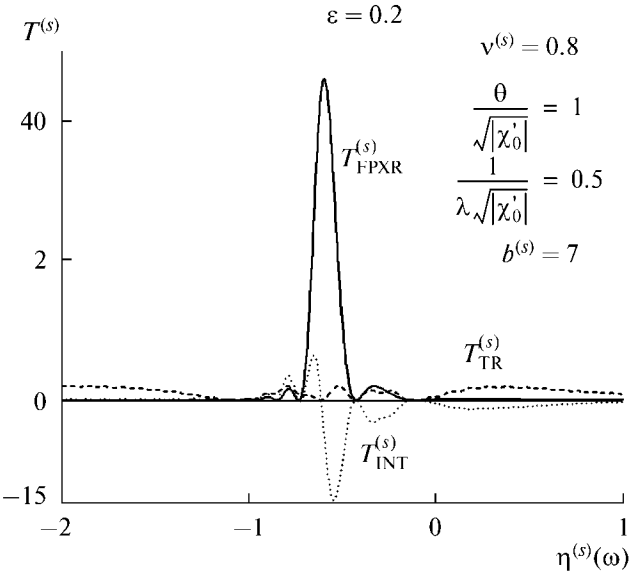

Fig. 12. Relative contributions similar to those in Fig. 11 in the case of asymmetric reflection.

ing observation angle θ, as shown in Fig. 8. However, in this case, the total radiation yield substantially decreases. It follows from Fig. 8 that the interference can substantially decrease the TR contribution into the total radiation spectrum.

Since the TR contribution into the total radiation spectrum (Fig. 6) insignificantly changes with decrease in asymmetry parameter ε, in contrast to the FPXR contribution (Fig. 4), it is of interest to consider the case where the asymmetry parameter is fairly large. The corresponding curves, which were calculated for the same values of parameters as in Figs. 7 and 8, are presented in Figs. 9 and 10. It is seen that the relative contribution of FPXR into the total radiation spectrum substantially increases and becomes dominant for sufficiently large observation angles. In addition, the interference between TR and FPXR is insignificant as well.

Since condition of TR suppression (8) can hardly be fulfilled in the real experiment, it is of interest to

estimate radiation contributions for an arbitrary thickness of the crystalline plate. Curves constructed according to formulas (9)–(11) are presented in Figs. 11 and 12. It is seen that the FPXR contribution to the total radiation spectrum is practically inconspicuous in the case of symmetric reflection (Fig. 11) and becomes dominant in the case of fairly strong asymmetry.

Thus, in the case of strong asymmetry, the target corresponding to the third diagram in Fig. 2 ($\varepsilon < 1$) makes it possible to observe the pronounced dynamic effect of FPXR on the background of transition radiation.

CONCLUSIONS

The analytic expressions for the spectral-angular distribution of coherent X-radiation emitted by a relativistic electron in the direction of its velocity during propagation through a single-crystal plate have been investigated. These expressions, which describe the contributions of forward diffracted parametric X-radiation (FPXR), transition radiation (TR), and their interference, have been derived in a two-wave approximation of the dynamic diffraction theory in the general case of asymmetric (with respect to the target surface) reflection of relativistic electron field. It is shown that both the FPXR spectrum amplitude and its angular density substantially increase with decreasing asymmetry parameter ε (Fig. 2). It is shown that the shape of the transition radiation peak likewise depends on the reflection asymmetry parameter owing to its influence on the ratio between the phase of the TR wave formed on the input surface of a crystalline plate (after the dynamic diffraction in the crystal) and the phase of the TR wave emitted from the output surface of a crystalline target. The relative contributions of FPXR and TR into the total radiation yield and the influence of their interference have been analyzed. It is shown that a decrease in asymmetry parameter ε leads to a growth in relative contribution of FPXR for both large and small observation angles. In the case of certain strong asymmetry, the contribution of FPXR becomes dominant.

REFERENCES

1. M. L. Ter-Mikaelyan, *The Influence of the Medium on High-Energy Electromagnetic Processes* (AN ArmSSR, Yerevan, 1969) [in Russian].
2. G. M. Garibyan and Yan Shi, Zh. Eksp. Teor. Fiz. **61**, 930 (1971) [Sov. Phys. JETP **34**, 495 (1971)].
3. V. G. Baryshevskii and I. D. Feranchuk, Zh. Eksp. Teor. Fiz. **61**, 944 (1971) [Sov. Phys. JETP **34**, 502 (1971)].
4. G. M. Garibyan and Sh. Yan, Zh. Eksp. Teor. Fiz. **63**, 1198 (1972) [Sov. Phys. JETP **36**, 631 (1972)].
5. V. G. Baryshevsky and I. D. Feranchuk, Phys. Lett. A **57**, 183 (1976).
6. V. G. Baryshevsky and I. D. Feranchuk, J. Phys. **44**, 913 (1983).
7. C. L. Yuan Luke, P. W. Alley, A. Bamberger, et al., Nucl. Instrum. Methods. Phys. Res. A **234**, 426 (1985).
8. B. N. Kalinin, G. A. Naumenko, D. V. Padalko, et al., Nucl. Instrum. Methods Phys. Res. B **173**, 253 (2001).
9. G. Kube, C. Ay, H. Backe, N. Clawiter, et al., in *Proc. of the 5th Intern. Symp. on Radiation from Relativistic Electrons in Periodic Structures, Lake Aya, Altai Mountains, Russia, 2001*, p. 25.
10. H. Backe, N. Clawiter, Th. Doerk, et al., in *Proc. of the Intern. Symp. on Channeling-Bent Crystals-Radiation Processes* (Frankfurt am Main, Germany, 2003), p. 41.
11. A. N. Aleinik, A. N. Baldin, E. A. Bogomazova, et al., Pis'ma Zh. Eksp. Teor. Fiz. **80**, 447 (2004) [JETP Lett. **80**, 393 (2004)].
12. N. Imanishi, N. Nasonov, and K. Yajima, Nucl. Instrum. Methods Phys. Res. B **173**, 227 (2001).
13. A. S. Kubankin, N. N. Nasonov, V. I. Sergienko, and I. E. Vnukov, Nucl. Instrum. Methods Phys. Res. A **201**, 97 (2003).
14. N. Nasonov and A. Noskov, Nucl. Instrum. Methods Phys. Res. A **201**, 67 (2003).
15. A. Kubankin, N. Nasonov, and A. Noskov, in *Proc. of the 7th Intern. Russ.-Jpn. Symp. on Interaction of Fast Charged Particles with Solids* (Kyoto, Japan, 2002), p. 217.
16. S. Blazhevich and A. Noskov, Nucl. Instrum. Methods Phys. Res. B **252**, 69 (2006).
17. S. V. Blazhevich and A. V. Noskov, Nucl. Instrum. Methods Phys. Res. A **266**, 3770 (2008).
18. S. V. Blazhevich and A. V. Noskov, Nucl. Instrum. Methods Phys. Res. A **266**, 3777 (2008).
19. S. V. Blazhevich and A. V. Noskov, Izv. Vyssh. Uchebn. Zaved., Fiz. **50**, 48 (2007).
20. Z. G. Pinsker, *Dynamical Scattering of X-rays in Crystals* (Nauka, Moscow, 1974; Springer, Berlin, 1978).
21. S. V. Blazhevich and A. V. Noskov, Journal of Surface Investigation. X-ray, Synchrotron and Neutron Techniques **4**, no. 2, pp. 303–314.